Hindawi
Shock and Vibration
Volume 2021, Article ID 1483594, 12 pages
https://doi.org/10.1155/2021/1483594

Research Article

A Deep Learning Framework for Damage Assessment of Composite Sandwich Structures

Viviana Meruane,[1,2] **Diego Aichele**,[1] **Rafael Ruiz**,[3] **and Enrique López Droguett**[1]

[1]*Department of Mechanical Engineering, Universidad de Chile, Beauchef 851, Santiago, Chile*
[2]*Millennium Nucleus on Smart Soft Mechanical Metamaterials, Beauchef 851, Santiago, Chile*
[3]*Department of Civil Engineering, Universidad de Chile, Blanco Encalada 2002, Santiago, Chile*

Correspondence should be addressed to Viviana Meruane; vmeruane@ing.uchile.cl

Received 21 April 2021; Revised 10 June 2021; Accepted 21 June 2021; Published 1 July 2021

Academic Editor: Claudio Sbarufatti

The vibrational behavior of composite structures has been demonstrated as a useful feature for identifying debonding damage. The precision of the damage localization can be greatly improved by the addition of more measuring points. Therefore, full-field vibration measurements, such as those obtained using high-speed digital image correlation (DIC) techniques, are particularly useful. In this study, deep learning techniques, which have demonstrated excellent performance in image classification and segmentation, are incorporated into a novel approach for assessing damage in composite structures. This article presents a damage-assessment algorithm for composite sandwich structures that uses full-field vibration mode shapes and deep learning. First, the vibration mode shapes are identified using high-speed 3D DIC measurements. Then, Gaussian process regression is implemented to estimate the mode shape curvatures, and a baseline-free gapped smoothing method is applied to compute the damage images. The damage indices, which are represented as grayscale images, are processed using a convolutional-neural-network-based algorithm to automatically identify damaged regions. The proposed methodology is validated using numerical and experimental data from a composite sandwich panel with different damage configurations.

1. Introduction

The vibration characteristics of composite structures are sensitive to debonding. In particular, mode shape curvatures are extensively used to identify debonding regions in composite materials [1–4], and a greater damage localization accuracy is achieved as the number of measured degrees of freedom (DOFs) increases [1]. However, the number of DOFs that can be acquired simultaneously is largely restricted in conventional vibration measurement techniques. To overcome this limitation, high-speed digital image correlation (DIC) techniques have been implemented for full-field vibration measurements and damage assessment [3–5].

In general, the damage can be identified by examining the changes in the modes of the damaged structure with respect to the undamaged modes. However, modes from the damaged structures cannot always be matched to a corresponding "baseline" mode in the undamaged structure. This has driven the development of baseline-free damage-assessment algorithms, which include gapped smoothing (GS) [2, 6, 7] and wavelet-based [8] methods. In wavelet-based methods, a continuous or discrete wavelet transform is used to detect abrupt changes in the mode shape displacements or curvatures, which are related to damage. However, the accuracy of these methods is particularly sensitive to the family and order of the wavelets selected [9]. The GS method was initially proposed by Ratcliffe and Bagaria [6], who assumed that the undamaged mode shapes can be estimated using a smoothed version of the damaged mode shapes. Then, the damage indices are computed from the difference between the shapes of the undamaged and damaged curvature modes. This method has proven to be useful in different damage detection and localization applications, such as damage identification in

beams [10], beam-like structures [11], and plate-like structures [2, 4, 7, 12]. Yoon et al. [7] implemented the GS method with mode shape curvatures to assess damage in plate-like structures under the assumption that stiffness reductions are related to damage. Their method was successful in identifying delamination in experimental composite panels. Qiao et al. [2] investigated the application of three damage-assessment methodologies in composite laminates: the generalized fractal dimension, strain energy method, and GS. The experimental and numerical data of a composite panel with delamination were used to validate the proposed approach. The experimental panel was excited using lead-zirconate-titanate actuators, and the vibratory response was captured using a scanning laser vibrometer with polyvinylidene fluoride sensors. In this case, the best results were obtained using the GS method. A principle similar to that of the GS method was used by Rucevskis et al. [12] to detect damage in plates. In their implementation, the damage indices were formulated as the difference between the measured mode shape curvatures of the damaged and undamaged panels. The undamaged mode-shaped curvatures were estimated using a smooth polynomial version of the damaged modes. The algorithm was investigated using the simulated data of a panel under different damage scenarios, considering the damage size, measurement noise, and sensor distribution. Then, the experimental data of an aluminum panel with a cut as the damage were employed to validate the approach.

Second-order displacement derivatives required to determine mode shape curvatures are frequently computed using the central difference method, which greatly amplifies the experimental noise. Another approach to obtain derivatives without noise amplification is by using Gaussian process (GP) regression models [13], which are effective nonparametric regression techniques [14]. Meruane et al. [4] combined the GS method with curvature mode shapes estimated through GP regression. They demonstrated that GP regression allows to obtain noise-free mode shape curvatures from mode shape displacements with noise, thus improving the damage identification results compared to those using the conventional GS method.

Previous methods, such as wavelet-based or GS methods, have been implemented to calculate damage indices distributed over the surface of a structure. Given the damage indices, the range of damage index values corresponding to the damaged and undamaged states must be determined. This can be viewed as a semantic segmentation problem, where each pixel must be classified as damaged or undamaged. The most straightforward solution is to use a statistical approach [3] under the assumption that the damage indices in the undamaged regions follow a normal statistical distribution. Therefore, the outliers were considered as damage indices corresponding to statistically significant characteristics, such as damaged elements. Alternatively, automatic thresholding techniques can be implemented, which are frequently used for the automated visual inspection of defects. The valley-emphasis method has been demonstrated to be particularly effective for damage assessment [4]. Unlike the statistical approach, this method automatically performs image segmentation without requiring parameter tuning. Recently, the introduction of deep learning techniques has generated tremendous progress in semantic segmentation. In particular, convolutional neural networks (CNNs) have obtained remarkable results for image segmentation [15], mainly because of their structure. That is, a CNN extracts relevant features from the input images in an incremental manner with no need for domain expertise. This allows the identification of hidden relationships in the images not evident to the naked eye, in many cases exceeding human precision. However, the application of CNNs for the identification of delaminated regions in composite panels has not yet been investigated.

This article presents a novel damage-assessment algorithm for composite sandwich structures based on full-field vibration mode shapes and deep learning. First, the vibration mode shapes were identified from high-speed DIC displacement measurements. Then, the curvature mode shapes were computed using a GP regression, and a baseline-free GS method was applied to compute the damage indices. The damage indices, which are represented as grayscale images, were processed using a CNN-based algorithm to identify the damaged regions automatically. The proposed methodology was validated using numerical and experimental data from a composite sandwich panel under different damage scenarios. Furthermore, to highlight the advantages of our approach over existing methods, the results obtained were compared with those of a similar approach that uses an automatic thresholding technique instead of a CNN for image segmentation [4].

2. Estimation of Curvatures Using GP Regression

The use of the GS technique requires the estimation of the curvatures of the damaged plates. This task is generally realized by applying a finite difference technique on the identified experimental vibration mode, thus making it susceptible to noise in the vibration modes. In this study, the use of a GP to estimate the plate's curvature is motivated by two main reasons: (1) GP can clean the noise from each vibration mode and (2) offer a smooth estimation of the second derivative (with the use of a squared exponential kernel).

Let us define the grid point coordinates using vector $\mathbf{X} = [(x_1, y_1), (x_2, y_2), \ldots, (x_n, y_n)]$and the measured mode shape displacements as $\phi_r = [\phi_r(x_1, y_1), \phi_r(x_2, y_2), \ldots, \phi_r(x_n, y_n)]$. The root mean square normalization is implemented as follows:

$$\varphi_r(x_i, y_j) = \phi_r(x_i, y_j) \sqrt{\frac{N_x N_y}{\sum_{i=1}^{N_x} \sum_{j=1}^{N_y} \phi_r^2(x_i, y_j)}}, \quad (1)$$

where N_x and N_y correspond to the number of grid points in the x and y directions, respectively, and $\varphi_r(x_i, y_j)$is the normalized r^{th} mode shape at points (x_i, y_j). Because the mode shape displacements include experimental noise, they can be expressed as

$$\varphi_r(x_i, y_i) = f(x_i, y_i) + \varepsilon, \tag{2}$$

where ε represents additive Gaussian noise, with a mean of 0 and variance σ_n^2. The mean mode shape displacements at points $(x_*, y_*)$are predicted as

$$\varphi_r^s(x_*, y_*) = \mathbf{k}_*^{\mathrm{T}}\mathbf{K}^{-1}\phi_r, \tag{3}$$

where $\mathbf{k}_*$ contains the kernel values between point $(x_*, y_*)$and grid points $\mathbf{X}$:

$$\mathbf{k}_*[i] = k((x_*, y_*), (x_i, y_i)). \tag{4}$$

Function k is the GP autocorrelation function. In this study, as in [4], a squared exponential kernel with additive noise was used:

$$k\left((x_i, y_i), \left(x_j, y_j\right)\right) = e^{-(1/2)\left(\left(\left(x_i - x_j\right)^2/s_x^2\right) + \left(\left(y_i - y_j\right)^2/s_y^2\right)\right)} + \sigma_n^2\delta_{ij}, \tag{5}$$

where $s_x^2$and $s_y^2$are the length scales that define the correlation between grid points, which ultimately drives the smoothness of the mode shape. Parameter σ_n^2accounts for the covariate noise and corresponds to the Kronecker delta. The selection of the squared exponential kernel is motivated by the need to have a GP that could be at least twice differentiable (to allow curvature estimation in damaged plates). $\mathbf{K}$ is the kernel matrix evaluated at the grid points and is defined as

$$\mathbf{K}[i, j] = k\left((x_i, y_i), \left(x_j, y_j\right)\right). \tag{6}$$

The mode shape curvatures are computed as

$$\begin{aligned}\frac{\partial^2\varphi_r^s(x_*, y_*)}{\partial x^2} &= \left[\mathbf{k}_{*xx}\right]^{\mathrm{T}}\mathbf{K}^{-1}\phi_r,\\ \frac{\partial^2\varphi_r^s(x_*, y_*)}{\partial y^2} &= \left[\mathbf{k}_{*yy}\right]^{\mathrm{T}}\mathbf{K}^{-1}\phi_r.\end{aligned} \tag{7}$$

Vectors $\mathbf{k}_{*xx}$and $\mathbf{k}_{*yy}$contain the second-order derivatives of the autocorrelation function evaluated at points $(x_*, y_*)$and grid point $\mathbf{X}$. Finally, the damage-assessment algorithm utilizes the mode shape Laplacian, which is formulated as

$$\nabla^2\varphi_r\left(x_i, y_j\right) = \frac{\partial^2\varphi_r^s\left(x_i, y_j\right)}{\partial x^2} + \frac{\partial^2\varphi_r^s\left(x_i, y_j\right)}{\partial y^2}. \tag{8}$$

3. GS Method

In the GS method, the undamaged mode shape curvatures are calculated using a smoothed version of the damaged mode shape curvatures (Laplacian). The undamaged mode shape curvatures are approximated using first-order base functions, as follows:

$$\nabla^2\varphi_r\left(x_i, y_j\right) = \mathbf{g}_{i,j}^{\mathrm{T}}\boldsymbol{\theta}_{i,j}, \tag{9}$$

where $\mathbf{g}_{i,j}$is a vector of base functions and $\theta_{i,j}$denotes its coefficients:

$$\begin{aligned}\mathbf{g}_{i,j}^{\mathrm{T}} &= \left[1, x_i, y_j\right],\\ \boldsymbol{\theta}_{i,j}^{\mathrm{T}} &= \left[a_0, a_1, a_2\right].\end{aligned} \tag{10}$$

Let us consider the neighboring points of (x_i, y_j); then, (9) can be expressed in the matrix form as follows:

$$\boldsymbol{\lambda}_r\left(x_i, y_j\right) = \mathbf{G}_r^{\mathrm{T}}\left(x_i, y_j\right)\theta_{i,j}, \tag{11}$$

where

$$\begin{aligned}\boldsymbol{\lambda}_r^{\mathrm{T}}\left(x_i, y_j\right) &= \left[\nabla^2\varphi_r\left(x_{i-1}, y_{j-1}\right), \nabla^2\varphi_r\left(x_i, y_{j-1}\right),\right.\\ &\qquad \left.\nabla^2\varphi_r\left(x_{i+1}, y_{j-1}\right), \ldots, \nabla^2\varphi_r\left(x_{i+1}, y_{j+1}\right)\right],\\ \mathbf{G}_r^{\mathrm{T}}\left(x_i, y_j\right) &= \left[\mathbf{g}_{i-1,j-1}, \mathbf{g}_{i,j-1}, \mathbf{g}_{i+1,j-1}, \ldots, \mathbf{g}_{i+1,j+1}\right].\end{aligned} \tag{12}$$

The coefficients are estimated using least squares resulting in

$$\widehat{\theta}_{i,j}^r = \left(\mathbf{G}_r^{\mathrm{T}}\left(x_i, y_j\right)\mathbf{G}_r\left(x_i, y_j\right)\right)^{-1}\mathbf{G}_r^{\mathrm{T}}\left(x_i, y_j\right)\boldsymbol{\lambda}_r\left(x_i, y_j\right). \tag{13}$$

These coefficients are used to calculate the undamaged mode shape curvature as

$$C_r\left(x_i, y_j\right) = \mathbf{g}_{i,j}^{\mathrm{T}}\widehat{\theta}_{i,j}^r. \tag{14}$$

The measure of damage at point $(x_i, y_j)$is estimated by the difference in the curvatures of the undamaged and damaged modes, represented by damage index d_r:

$$d_r\left(x_i, y_j\right) = \left|\nabla^2\varphi_r\left(x_i, y_j\right) - C_r\left(x_i, y_j\right)\right|. \tag{15}$$

Ultimately, this expression is expanded to consider the first m modes:

$$d\left(x_i, y_j\right) = \sum_{r=1}^{m} d_r\left(x_i, y_j\right). \tag{16}$$

4. Deep Learning and Semantic Segmentation

Deep learning models have shown excellent performance in various tasks involving image recognition and computer vision, such as image classification [16, 17], natural language processing [18], and image segmentation [15]. In particular, CNNs have been extensively used for image classification, where the network output to an image is a class label. This is achieved by arranging convolutional, pooling, and fully connected layers, as illustrated in Figure 1.

The convolution operation utilizes weight matrix $\mathbf{K}$, denominated as a filter or kernel, to obtain feature matrix $\mathbf{S}$ from input matrix $\mathbf{A}$ as follows:

$$\mathbf{S} = \mathbf{A} * \mathbf{K}, \quad \text{where } \mathbf{S}(i, j) = \sum_n\sum_m \mathbf{A}(i - m, i - n)\cdot\mathbf{K}(m, n). \tag{17}$$

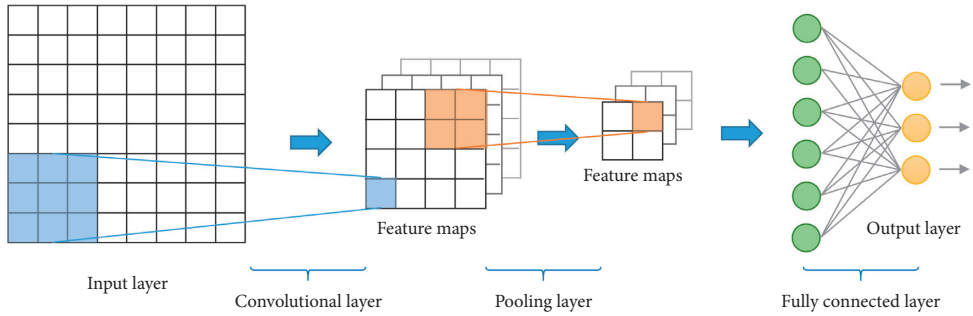

Figure 1: CNN architecture for image classification.

Then, the feature matrix is added to bias matrix **B**, and the activation function is employed to build the feature map **H**:

$$\mathbf{H} = f(\mathbf{A} * \mathbf{K} + \mathbf{B}). \tag{18}$$

The convolution layer applies various kernels and biases to the input matrix, and by operating convolutional layers sequentially, high-level features can be extracted. Pooling layers can then be used to reduce the number of features. For instance, a max-pooling layer provides only the maximum value of the next feature map within a rectangular cell. Finally, a feed-forward neural network located at the end of the CNN delivers the predicted class labels.

Considering the significant quantity of parameters in a CNN, precautions must be taken to prevent overfitting or overadjustment of the CNN to the training data. Overfitting results in an inadequate generalization; therefore, the network is unable to predict unseen cases. Regularization techniques, such as dropout [19] and batch normalization [20], can be implemented to prevent overfitting. In addition, the early stopping strategy, which stops training when the validation error begins to increase, helps prevent overfitting.

Although the most common application of a CNN is image classification, it has also been implemented for image segmentation. In image segmentation, the classification is performed pixel by pixel. Long et al. [21] were the first to introduce a fully CNN for image segmentation, in which the fully connected layers were replaced by convolutional layers. They used interpolation layers to guarantee that the output size equals the input size, which is essential for image segmentation. Ronneberger et al. [22] modified this architecture to allow training with fewer images, and the proposed architecture was named U-Net because of its shape, as illustrated in Figure 2.

The U-Net architecture is characterized by a contraction-expansion configuration. The contraction part is built by arranging convolutional layers using 3×3 kernels, rectified linear activation functions, and pooling layers. For a certain number of convolutional layers, max-pooling with stride 2 was implemented. The combination of a convolutional layer followed by max-pooling is a contraction step. In Figure 2, each contraction step is composed of two convolutional layers and one max-pooling layer; at each step, the number of channels (kernels) is doubled.

In the expansive part, the pooling layers are replaced by upsampling layers, which have the opposite purpose of pooling layers, thereby increasing the size of the input matrix. To increase the localization accuracy, features from the contracting part are joined to the features in the upsampled output. This is represented by the segmented lines in Figure 2. Finally, a 1×1 convolution layer is employed to transform the feature vectors to the required number of classes.

5. Damage-Assessment Methodology

The proposed damage-assessment methodology comprises the following steps:

(1) The experimental mode shapes are identified using a high-speed DIC system, as described in Section 5.3.

(2) The mode shape curvatures are estimated using a Gaussian regression process. The values of the length scale parameters ($s_x^2$and s_y^2) and the noise variance (σ_n^2)are the same as those used in [4] because the application case is the same: $s_x = s_y = 5d_x$and $\sigma_n^2 = 1$. As the GP is used merely to clean the noise from vibration modes and facilitate the curvature estimation, a robust selection of GP hyperparameters (s_x^2, s_y^2, σ_n^2) is considered unnecessary as long as the GP mean corresponds to the observations, i.e., no bias is introduced (which is demonstrated in [4] by studying the residual error). However, a new hyperparameter selection is recommended for new applications.

(3) Damage indices are obtained according to the procedure presented in Section 3.

(4) The damaged regions are identified using a CNN with a customized version of the U-Net architecture, which is presented in Section 6.1. The CNN was trained using a database created using a numerical model of the composite sandwich panel.

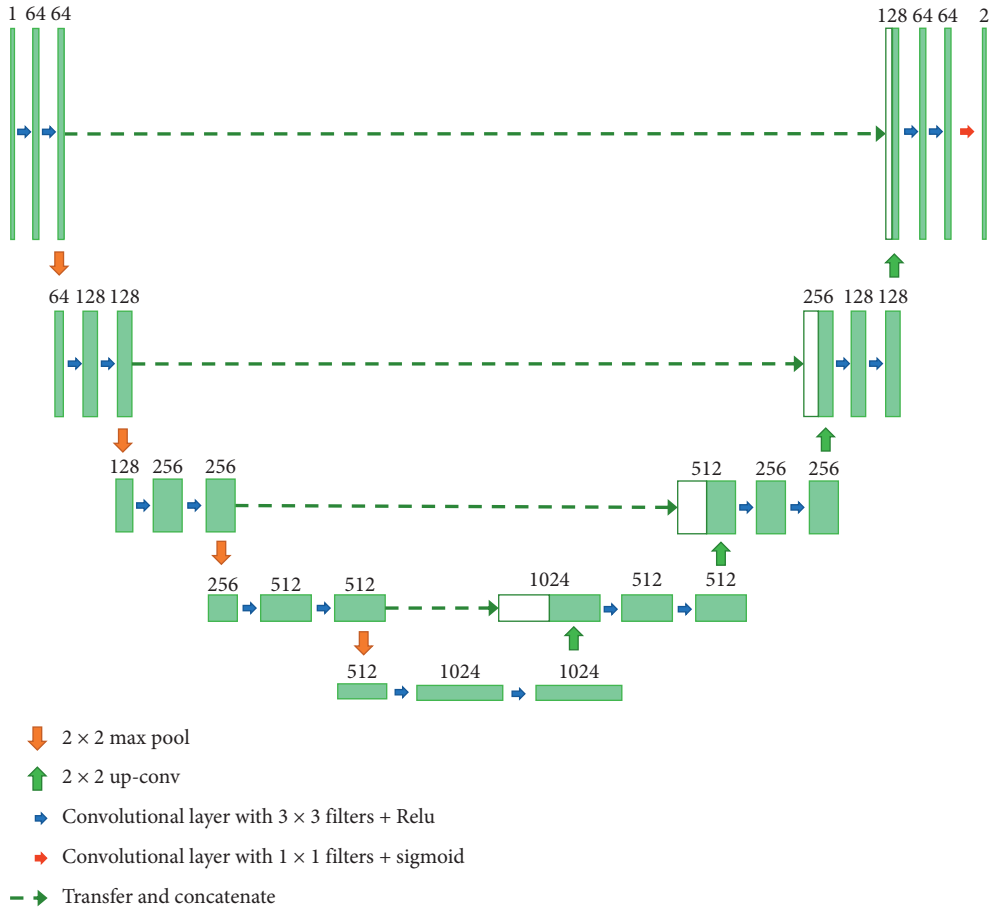

Figure 2: Scheme of the U-Net architecture.

This methodology was applied to identify debonding damage in an aluminum composite sandwich panel using numerical and experimental data. An automatic thresholding technique was used to contrast the image segmentation results obtained with the proposed approach.

The intersection over union (IoU) metric, which is widely used in image segmentation and object detection problems [23], was employed to evaluate the segmentation. In the damage identification problem, we have the true damaged region of the panel and the predicted damaged region, as illustrated in Figure 3. The true positives (TP) are defined as the intersection between both regions; false negatives (FN) correspond to the actual damage that was not detected, whereas the false positives (FP) were incorrectly detected damage. Considering this, the IoU metric is calculated as

$$\text{IoU} = \frac{\text{area of overlap}}{\text{area of union}} = \frac{\text{TP}}{\text{TP} + \text{FP} + \text{FN}}. \quad (19)$$

5.1. Application Case. An aluminum honeycomb sandwich panel with dimensions 0.35 m × 0.25 m × 0.021 m was used in our case study. The skins are made of aluminum sheets with 0.8 mm thickness and the properties listed in Table 1,

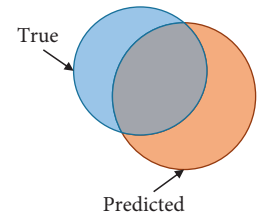

Figure 3: Representation of true and predicted damaged regions.

Table 1: Skin characteristics.

Thickness	0.8 mm
Elastic modulus	6.9×10^{10} Pa
Poisson's ratio	0.33
Density	2700 kg/m^3

Table 2: Core characteristics.

Cell size	19.1 mm
Foil thickness	5×10^{-5} m
Thickness	10 mm
Density	20.8 kg/m^3
Compressive strength	0.448 MPa
Longitudinal shear strength (σ_{xy})	0.345 MPa
Longitudinal shear modulus (G_{xy})	89.63 MPa
Transversal shear strength (σ_{yz})	0.241 MPa
Transversal shear modulus (G_{yz})	41.37 MPa

Figure 4: Experimental panel with speckle pattern.

Table 3: Experimental damage cases.

Case	Normalized damage size		Shape
	Damage 1	Damage 2	
1	0.09	—	Circular
2	0.12	—	Circular
3	0.14	0.07	Square
4	0.11	0.17	Circular

whereas the honeycomb core is made of aluminum with the characteristics presented in Table 2.

Figure 4 shows the experimental panel. For DIC measurements, the face of the panel was painted with a speckled pattern. The aluminum panel was built by bonding the skin to the honeycomb core with an epoxy resin. To introduce debonding damage to one of the skins, a region was intentionally left without an adhesive.

The panels were manufactured with four damage configurations, as listed in Table 3, describing the summary of the damage scenarios with the corresponding attributes, which include circular and square debonding damage shapes and a range of damage sizes. In the third and fourth cases, the panel has two debonded regions, whereas the first and second cases have one debonded region. The normalized damage size, which ranged from 0.07 to 0.17, is defined as the size of the damaged region (diameter or side length) divided by the diagonal length of the panel.

5.2. Numerical Model. The numerical model considers the composite panel as three layers of shell elements connected by linear springs. The exterior shells represent the skin, and the interior shell represents the honeycomb core. The springs act as the epoxy adhesive layer; therefore, the damaged region is represented as a zone with reduced spring stiffness. The model was built using the Structural Dynamics Toolbox (SDT) [24] using MATLAB®, and the layers were modeled with isotropic four-node shell elements (see Figure 5).

Experimental noise is always present in mode shapes identified from experimental data, which is why we decided to introduce noise artificially into the numerical mode shapes to make them similar to the experimental ones. In particular, the noise is introduced by adding a random sample to the mode amplitude at each grid point, where the samples are obtained from a Gaussian distribution with zero mean and standard deviation equal to 10% of the maximum mode amplitude. A database of 3500 panels with a range of damage scenarios was generated to train and evaluate the damage-assessment algorithms. The panels in the database had circular debonded regions with normalized damage sizes ranging between 0 and 0.25, and both the damage location and size were defined randomly.

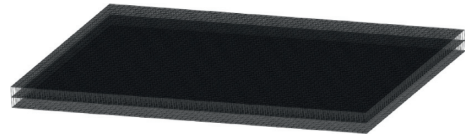

Figure 5: Numerical model representing the sandwich panel.

5.3. Experimental Setup and Measurements. Figure 6 presents the experimental setup, where the panel is suspended by elastic cords while it is excited by an electrodynamic shaker. The panel displacements were captured by two high-speed cameras connected to the DIC software. The DIC system is a Q450 high-speed DIC system manufactured by Dantec Dynamics. The acquisition frequency was 7530 fps and the picture resolution was 1 MP.

The experimental mode shapes are identified according to the following procedure:

(1) First, the natural frequencies of the panel are identified by an impact test

(2) The shaker is configured to vibrate with a sinusoidal signal at the natural frequency

(3) The panel vibration is recorded with the cameras, and the displacements are calculated using the DIC software

(4) The displacements are exported to MATLAB, and the operational mode shapes are identified

(5) Steps 2 to 4 are repeated for each natural frequency

Mode shapes with frequencies up to 2000 Hz were identified, and the number of experimental modes in this frequency range varied between 6 and 11 for each panel.

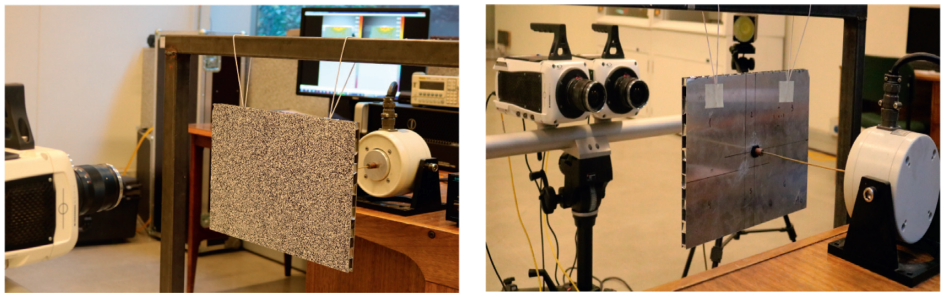

(a) (b)

Figure 6: Experimental setup: (a) panel with the speckle pattern and (b) shaker attachment.

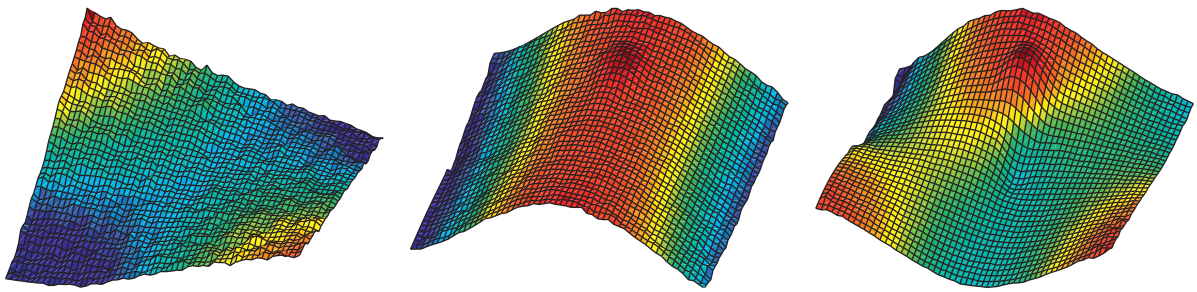

(a) (b) (c)

Figure 7: Example of the first three experimental mode shapes. (a) 488 Hz. (b) 612 Hz. (c) 968 Hz.

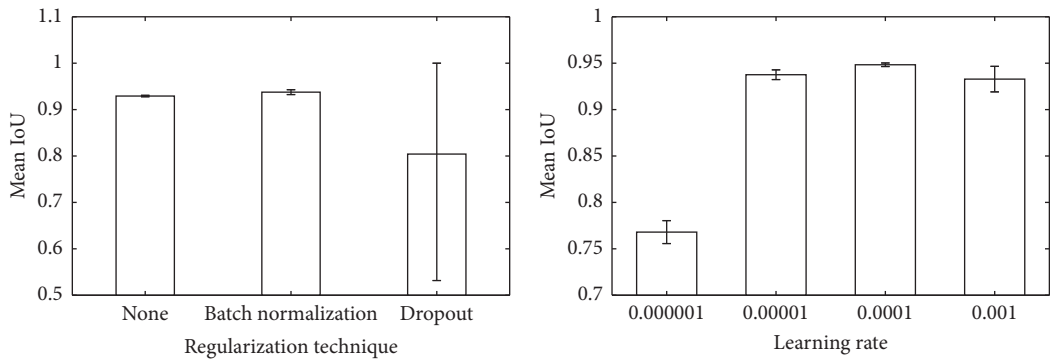

(a) (b)

Figure 8: Validation performance with different (a) regularization strategies and (b) learning rates.

Figure 7 illustrates the first three experimental modes obtained for the first panel (Case 1).

6. Results

The numerical database was divided into training, validation, and testing sets. A total of 2800 panels were used for training, 175 for validation, and 525 for testing. The validation set was used during training and to tune the model, whereas the testing set was used to test the final model.

6.1. Optimization of Model Parameters. The first test was performed using the standard U-Net architecture, as described in Section 4. The algorithm was initially trained using the Adam optimizer, and the learning rate was set to 0.00001. The loss function was defined as (1 – IoU). An early stopping strategy was adopted with a validation patience of 50 epochs. Therefore, if the validation loss did not improve after 50 epochs, the training was stopped. To define the best regularization strategy, three cases were evaluated: no regularization, batch normalization, and

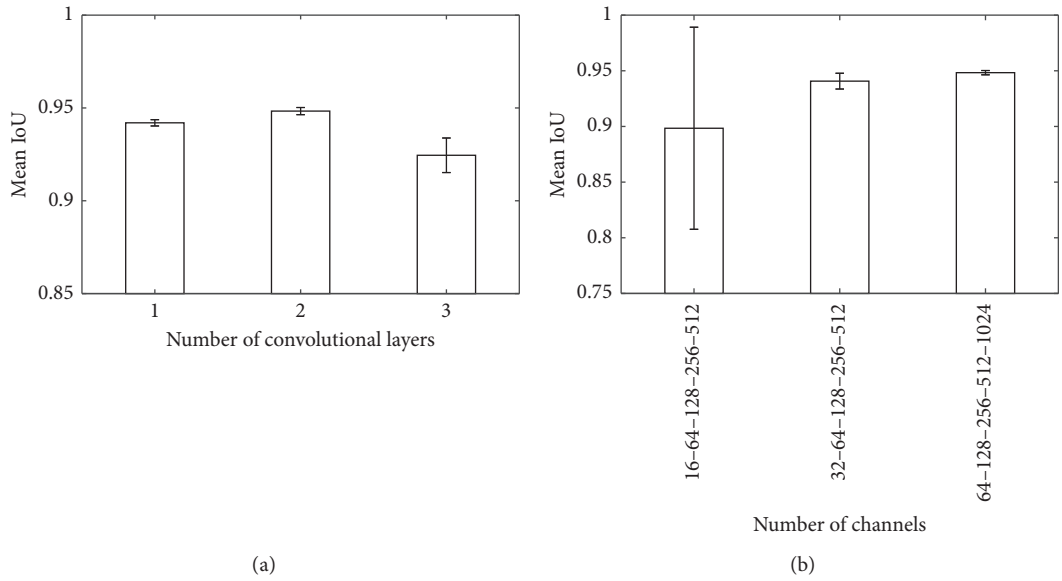

Figure 9: Validation performance with respect to the (a) number of convolutional layers and (b) number of channels.

Table 4: Segmentation model configuration.

Optimizer	Adam
Learning rate	0.0001
Regularization strategy	Batch normalization
Model architecture	U-Net
Number of channels	64–128–256–512–1024
Number of convolutional layers per step	2

dropout (20%). Because variability exists in each training process, each case was trained five times. Figure 8(a)shows the mean validation IoU obtained in each case, and the error bars represent the standard deviation. The best performance was obtained by batch normalization. Therefore, this regularization strategy was adopted. Next, a sensitivity analysis was performed with respect to the learning rate. The results shown in Figure 8(b)indicate that the best learning rate is 0.0001.

Finally, two additional sensitivity analyses were conducted. The first analysis explored the optimal number of convolutional layers at each step of the U-Net algorithm. In the second analysis, the optimal number of channels was investigated. The results are illustrated in Figure 9, and the final configuration of the deep learning segmentation model is summarized in Table 4.

6.2. Numerical Damage Assessment. Figure 10 shows the damage-assessment performance of the testing data as a function of the normalized damage size. The results were compared with the results obtained using an automatic thresholding method, as described in [4]. The results clearly indicate that by using a CNN for segmentation, the damage is identified with a significantly higher exactitude, which allows for the detection of smaller-sized damages.

Some examples of damage identified by both approaches are shown in Figure 11. The damage indices tended to increase at the edges of the panels. This effect is most clearly observed in cases with small damage sizes. Indeed, in cases with small or no damage, larger damage indices are at the edges. This causes the automatic thresholding method to identify damage incorrectly at the edges, but the CNN-based approach is capable of learning that these indices on the edges do not correspond to damage. Furthermore, the CNN is capable of detecting damages as small as a 0.05 normalized size. Damage of this size is not discerned by the human eye in the damage index image or by the thresholding methods.

The automatic thresholding method merely finds regions where the damage indices exceed a certain threshold and identifies those regions as damaged. In contrast, the CNN-based approach can learn different damage index patterns and identify whether an increase in damage indices corresponds to actual damage. This enables the identification of small damages that are not identifiable with other methods and prevents the detection of false damage.

6.3. Experimental Damage Assessment. To validate the approach with the experimental data, four experimental damage scenarios were considered, as listed in Table 1. The damage identified using the proposed CNN-based methodology is shown in Figure 12, whereas the results of the automatic thresholding method are presented in Figure 13. Table 5 summarizes the IoU obtained using the proposed approach compared to the IoU obtained using the automatic thresholding method. On average, the CNN approach performs better, although it is not a significant improvement. The main advantage of the CNN-based approach is that it does not detect false damages and can detect small damages. For example, the CNN-based approach correctly identified the smaller-sized damage in Case 3, but the

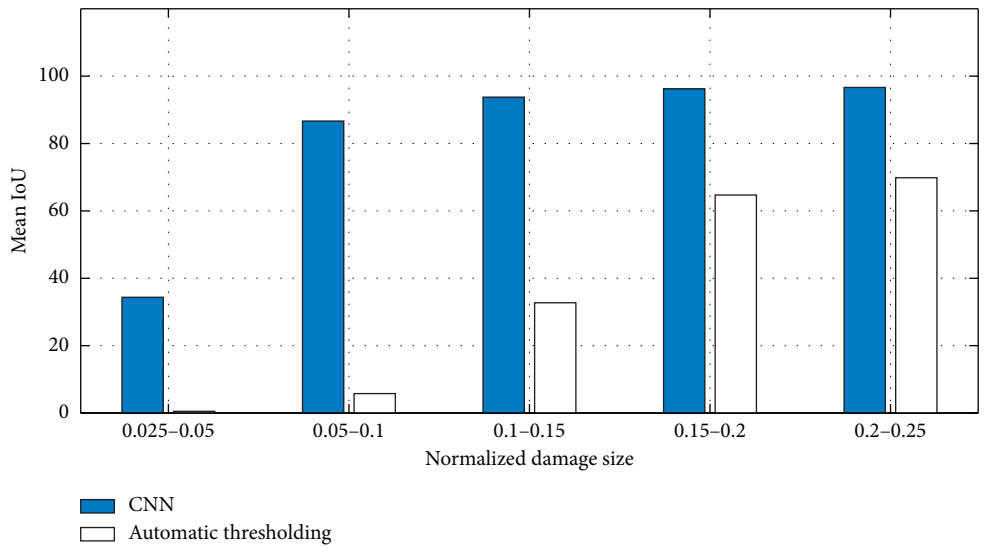

Figure 10: Performance of the damage-assessment methodologies.

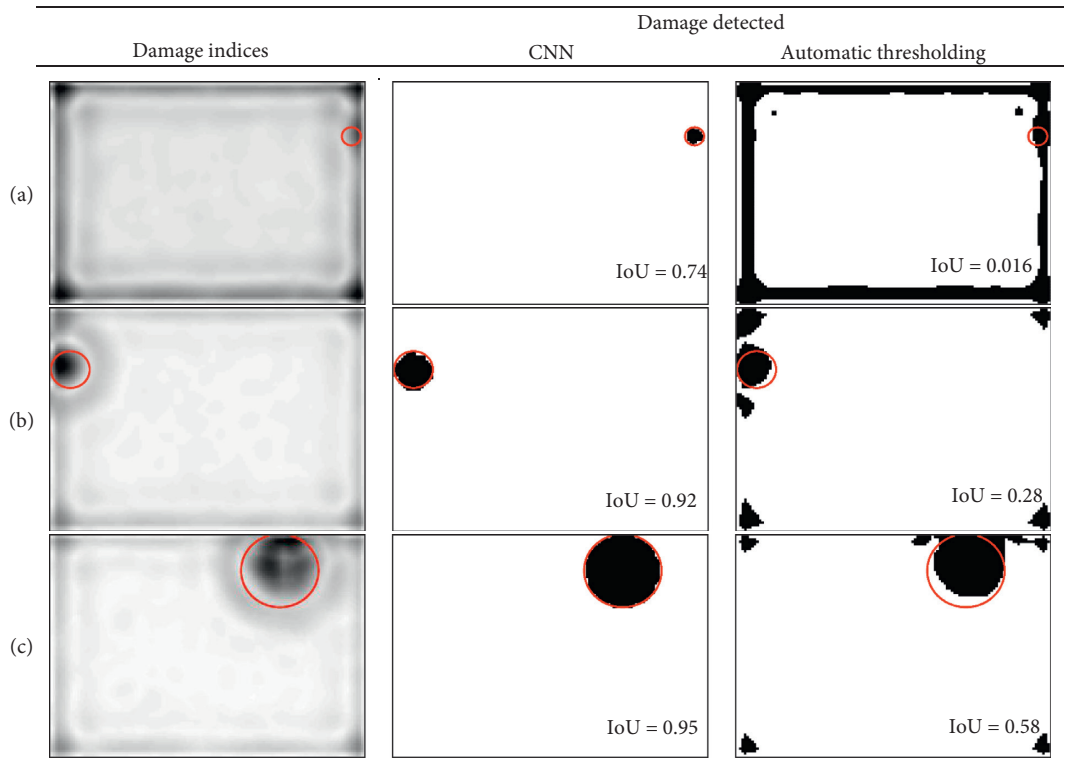

Figure 11: Damage detected using CNN and automatic thresholding method. Normalized damage sizes: (a) 0.05, (b) 0.1, and (c) 0.2. The red circles indicate the true damage.

automatic thresholding method did not. Thus, the automatic thresholding method performed satisfactorily in Case 3 because this model can catch the bigger damages very well, but it misses the small ones completely. Conversely, the CNN-based method is much better at identifying small damages. Furthermore, the experimental investigation indicates that the proposed approach is capable of correctly generalizing the numerical data because it accurately detects

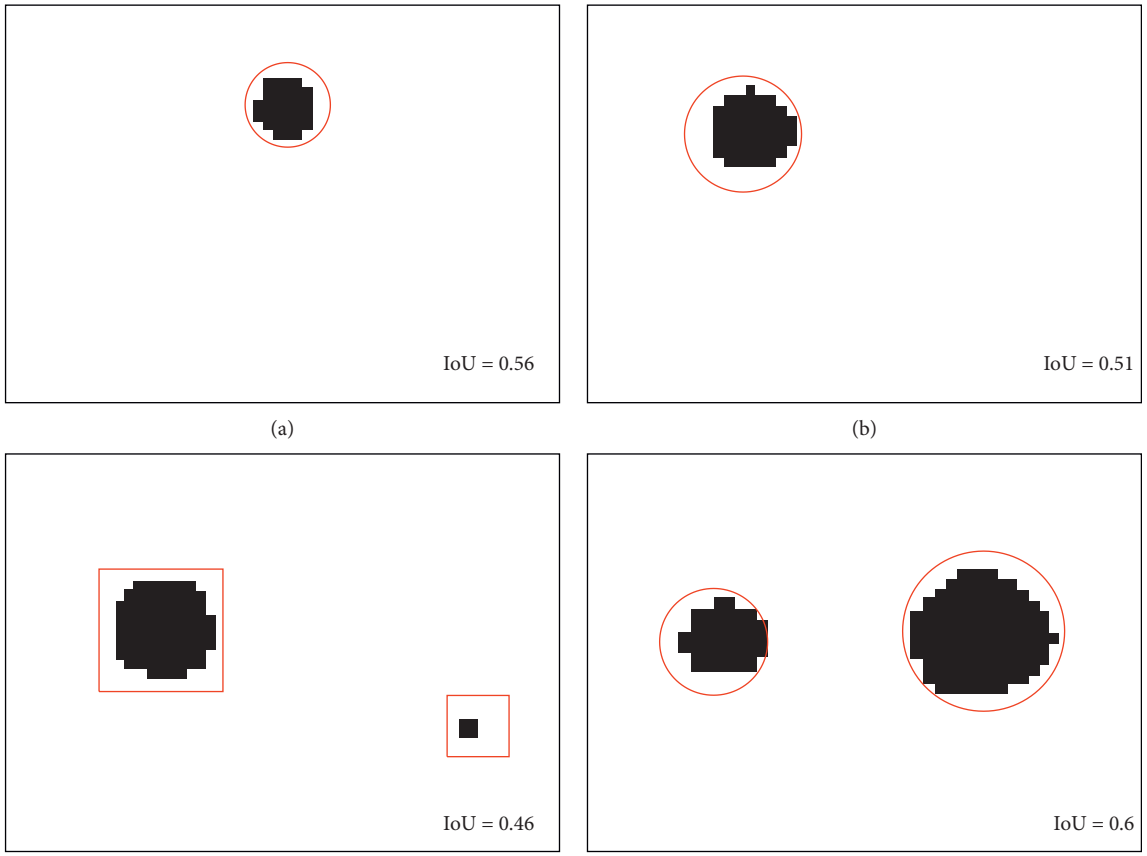

Figure 12: Experimental damage identified with the proposed CNN-based approach. Normalized damage sizes: (a) 0.09 (Case 1), (b) 0.12 (Case 2), (c) 0.14 and 0.07 (Case 3), and (d) 0.11 and 0.17 (Case 4). The red circles/squares denote the true damage region.

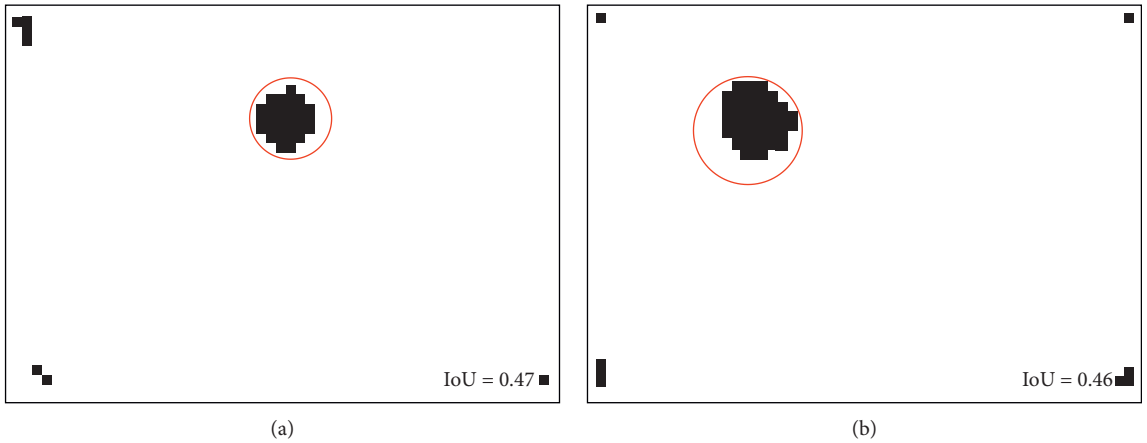

Figure 13: Continued.

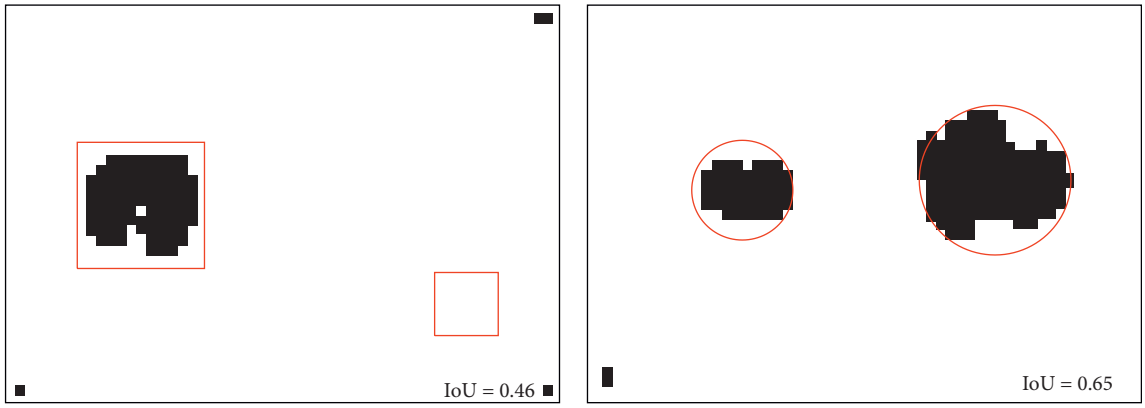

(c) (d)

Figure 13: Experimental damage identified with an automatic thresholding method. Normalized damage sizes: (a) 0.09 (Case 1), (b) 0.12 (Case 2), (c) 0.14 and 0.07 (Case 3), and (d) 0.11 and 0.17 (Case 4). The red circles/squares denote the true damage region.

Table 5: Performance of the damage detected using CNN and automatic thresholding method.

Case	IoU	
	CNN	Automatic thresholding
1	0.56	0.47
2	0.51	0.46
3	0.46	0.46
4	0.60	0.65

experimental damage with precision despite having been trained using only data from the numerical model.

7. Conclusions

A damage-assessment methodology using full-field vibration modes and deep learning was developed and implemented to assess the debonding damage in composite sandwich structures. The main novelty of this approach is that the damage indices, represented as grayscale images, are processed using a CNN to automatically identify the damaged regions. The results showed that, compared with automatic thresholding methods, the CNN can better identify damaged regions with respect to IoU. In particular, the CNN enables the identification of smaller damages, significantly improving the results of existing approaches; this is essential from a practical perspective.

The proposed approach can learn different damage index patterns and correctly identify whether an increase in damage indices corresponds to actual damage. This advancement enables the identification of damage that is too small to be identified by other methods and prevents the detection of false damage. The results indicate that the proposed approach can correctly assess damages with normalized sizes greater than 0.05.

Although the experimental results are encouraging, the number of cases studied is not statistically significant, and therefore further experimental analysis is required. In addition, the proposed approach was validated using a simple sandwich plate structure. This structure does not necessarily represent a real structure with geometrical changes and different types of joints and edge conditions. Therefore, applications with more complex and realistic structures will be investigated in the future. In particular, the effects of different boundary conditions and geometrical changes on the damage identified must be analyzed. Because the approach searches for discontinuities in the structure, it is important to discriminate between changes caused by damage and variations due to geometry or boundary conditions.

Data Availability

Experimental and numerical data used in this article are available for download in the following website: http://www.lvmr.cl/des_en.htm.

Conflicts of Interest

The authors declare that there are no conflicts of interest.

Acknowledgments

The authors acknowledge the financial support provided by the Chilean National Fund for Scientific and Technological Development (FONDECYT) under grant nos. 1170535 and 1190720 and the Millennium Science Initiative of the Ministry of Economy, Development, and Tourism, grant "Millennium Nucleus on Smart Soft Mechanical Metamaterials."

References

[1] P. M. García, J. V. A. D. Santos, and H. Lopes, "A new technique to optimize the use of mode shape derivatives to localize damage in laminated composite plates," *Composite Structures*, vol. 108, no. 1, pp. 548–554, 2014.

[2] P. Qiao, K. Lu, W. Lestari, and J. Wang, "Curvature mode shape-based damage detection in composite laminated plates," *Composite Structures*, vol. 80, no. 3, pp. 409–428, 2007.

[3] F. Seguel and V. Meruane, "Damage assessment in a sandwich panel based on full-field vibration measurements," *Journal of Sound and Vibration*, vol. 417, pp. 1–18, 2018.

[4] V. Meruane, I. Fernandez, R. O. Ruiz, G. Petrone, and D. E. Lopez, "Gapped Gaussian smoothing technique for debonding assessment with automatic thresholding," *Structural Control Health Monitoring*, vol. 26, 2019.

[5] V. Meruane, M. Lasen, E. L. Droguett, and A. O Bernardin, "Modal strain energy-based debonding assessment of sandwich panels using a linear approximation with maximum entropy," *Entropy*, vol. 19, no. 11, pp. 619–622, 2017.

[6] C. P. Ratcliffe and W. J. Bagaria, "Vibration technique for locating delamination in a composite beam," *AIAA Journal*, vol. 36, no. 6, pp. 1074–1077, 1998.

[7] M. K. Yoon, D. Heider, J. W. Gillespie, C. P. Ratcliffe, and R. M. Crane, "Local damage detection using the two-dimensional gapped smoothing method," *Journal of Sound and Vibration*, vol. 279, no. 1-2, pp. 119–139, 2005.

[8] C. C. Chang and L. W. Chen, "Damage detection of a rectangular plate by spatial wavelet based approach," *Applied Acoustics*, vol. 65, no. 8, pp. 819–832, 2004.

[9] A. Katunin, "Stone impact damage identification in composite plates using modal data and quincunx wavelet analysis," *Archives of Civil and Mechanical Engineering*, vol. 15, no. 1, pp. 251–261, 2015.

[10] C. P. Ratcliffe, "Damage detection using a modified laplacian operator on mode shape data," *Journal of Sound and Vibration*, vol. 204, no. 3, pp. 505–517, 1997.

[11] A. K. Pandey, M. Biswas, and M. M. Samman, "Damage detection from changes in curvature mode shapes," *Journal of Sound and Vibration*, vol. 145, no. 2, pp. 321–332, 1991.

[12] S. Rucevskis, R. Janeliukstis, P. Akishin, and A. Chate, "Mode shape-based damage detection in plate structure without baseline data," *Structural Control and Health Monitoring*, vol. 23, no. 9, pp. 1180–1193, 2016.

[13] C. E. Rasmussen, "Gaussian processes in machine learning," in *Advanced Lectures on Machine Learning*Springer, Berlin, Germany, 2004.

[14] J. Ko and D. Fox, "GP-BayesFilters: bayesian filtering using Gaussian process prediction and observation models," *Autonomous Robots*, vol. 27, no. 1, pp. 75–90, 2009.

[15] Y. Guo, Y. Liu, T. Georgiou, and M. S. Lew, "A review of semantic segmentation using deep neural networks," *International Journal of Multimedia Information Retrieval*, vol. 7, no. 2, pp. 87–93, 2018.

[16] W. Rawat and Z. Wang, "Deep convolutional neural networks for image classification: a comprehensive review," *Neural Computation*, vol. 29, no. 9, pp. 2352–2449, 2017.

[17] C. Modarres, N. Astorga, E. L. Droguett, and V. Meruane, "Convolutional neural networks for automated damage recognition and damage type identification," *Structural Control and Health Monitoring*, vol. 25, no. 10, 2018.

[18] T. Young, D. Hazarika, S. Poria, and E. Cambria, "Recent trends in deep learning based natural language processing [review article]," *IEEE Computational Intelligence Magazine*, vol. 13, no. 3, pp. 55–75, 2018.

[19] S. Wager, S. Wang, and P. S. Liang, "Dropout training as adaptive regularization," *Advances in Neural Information Processing Systems*, Stanford University, Stanford, CA, USA, 2013.

[20] S. Ioffe and C. Szegedy, "Batch normalization: accelerating deep network training by reducing internal covariate shift," 2015, https://arxiv.org/abs/1502.03167.

[21] J. Long, E. Shelhamer, and T. Darrell, "Fully convolutional networks for semantic segmentation," in *Proceedings of the IEEE Conference on Computer Vision and Pattern Recognition*, pp. 3431–3440, Boston, MA, USA, June 2015.

[22] O. Ronneberger, P. Fischer, and T. Brox, "U-net: convolutional networks for biomedical image segmentation," in *Proceedings of International Conference on Medical Image Computing and Computer-Assisted Intervention*, pp. 234–241, Munich, Germany, October 2015.

[23] M. A. Rahman and Y. Wang, "Optimizing intersection-over-union in deep neural networks for image segmentation," in *Proceedings of International Symposium on Visual Computing*, pp. 234–244, Las vegas, NV, USA, December-2016.

[24] E. Balmès, J. P. Bianchi, and J. M. Leclère, *Structural Dynamics Toolbox User's Guide*, SDTools, Paris, France, 2011.